

Detuning-induced stimulated Raman adiabatic passage in atoms with hyperfine structure

Li Deng and Takashi Nakajima*

Institute of Advanced Energy, Kyoto University, Gokasho, Uji, Kyoto 611-0011, Japan

(Received 3 December 2013; published 7 February 2014)

We theoretically study the generation of coherence in generalized two-level atoms with hyperfine structure by utilizing the detuning-induced stimulated Raman adiabatic passage (D-STIRAP). As expected, the degree of attainable coherence between the ground and excited states cannot be as large as that for the ideal two-level atoms without hyperfine structure. However, we find that the substantial degree of coherence can still be produced with small modulations, and the modulation period is essentially determined by the hyperfine splittings in the ground and excited states. The D-STIRAP scheme in generalized two-level atoms is sufficiently robust against the various parameters such as intensities of lasers, initial detuning, time delay between the laser pulses, and Doppler broadening. As a specific example, we show realistic results for the D_1 transition of Na.

DOI: [10.1103/PhysRevA.89.023406](https://doi.org/10.1103/PhysRevA.89.023406)

PACS number(s): 32.80.Qk, 33.80.Be, 42.50.Ct

I. INTRODUCTION

Studies on atomic coherence have drawn a lot of attention for decades. Atomic coherence can be utilized in many interesting and important phenomena such as electromagnetically induced transparency (EIT) [1], lasing without inversion (LWI) [2], and stimulated Raman adiabatic passage (STIRAP) [3]. It also plays an essential role in the currently popular area of quantum information [4].

Atomic coherence can also be utilized to enhance the conversion efficiency of various nonlinear optical processes such as four-wave mixing (FWM). For instance, maximum coherence prepared between the two ground states in Λ or double- Λ systems results in high conversion efficiency of the FWM field within one coherence length, which means that the phase matching condition is not required for the efficient FWM processes [5–7]. Similarly, large coherence prepared between the ground and highly excited states can lead to the enhancement of FWM processes in the vacuum ultraviolet (VUV) or extreme ultraviolet (XUV) regions [8–15], which is known to be a very difficult task [16–19].

Due to the broad applications such as those mentioned above, many different schemes have been proposed to optically control the generation of atomic coherence. For instance, there are a variety of choices [20–24] to prepare large coherence between two ground states. Nevertheless, there is no concrete scheme known to produce large coherence between the ground and highly excited states, which is a key to efficiently generate the VUV-XUV light through FWM. The resonant two-photon excitation scheme, which is the simplest for this purpose, suffers from the strict requirements on the pulse intensity and frequency. This means that the Doppler broadening can easily spoil the conversion efficiency of FWM processes.

Recently a much more robust scheme has been proposed to generate coherence between the ground and excited states [25], which has also been studied earlier in Ref. [26] in a slightly different context. It is a variant of the ordinary STIRAP scheme, and we call it D-STIRAP (detuning-induced STIRAP). The D-STIRAP scheme is shown in Fig. 1. The essence of the D-STIRAP scheme is that the Bloch equations for a

two-level system, which consists of the three variables, is mathematically similar to the Schrödinger equations for a three-level Λ system. In the standard STIRAP scheme (with a three-level Λ system), a complete population transfer will occur from the initially occupied ground state to the initially unoccupied third state if the pump and Stokes pulses interact with atoms in the counterintuitive pulse sequence, while in the D-STIRAP scheme, stable and maximum coherence will be produced between the initially occupied lower and initially unoccupied upper states if the detuning pulse is turned on earlier than the pump pulse (see Fig. 1). For this process to occur, the adiabatic condition $\int_{-\infty}^{\infty} \sqrt{\Delta^2 + \Omega^2} dt \gg \pi/2$ must be satisfied, in which Δ is the detuning and Ω is the Rabi frequency of the pump pulse. The process can be realized by using a linearly chirped pump pulse [27] or transform-limited pump pulse together with an off-resonant Stark pulse [12] to induce dynamic detuning during the pump pulse. Related studies with the D-STIRAP scheme show that this scheme is not sensitive to pump pulse intensity, detuning, or the time delay between the two (Stark and pump) pulses [12,28], and consequently the Doppler broadening of the target atomic gas does not spoil the generation of high coherence [12].

In practice, however, it is not always easy to realize a two-level system. This is particularly true for the case in which pulsed lasers are employed: With a pulsed laser excitation a hyperfine structure cannot be easily resolved, as a result of which each lower and upper state consists of a few unresolved hyperfine sublevels. That is why there are many works which deal with the influence of the presence of hyperfine structure on various coherent control schemes [29–32] such as EIT and coherent population trapping (CPT).

The purpose of this paper is, with a similar spirit, to theoretically study the influence of hyperfine structure on the generation of coherence in generalized two-level atoms through the D-STIRAP scheme. To be most specific we consider the $3^2S_{1/2}$ and $3^2P_{1/2}$ states of ^{23}Na (nuclear spin = 3/2, natural abundance = 100%), each of which consists of hyperfine sublevels and associated magnetic sublevels. Starting from the formal derivation of time-dependent equations for the system of interest we recast them into the generalized Bloch equations. The generalized Bloch equations turn out to be very useful to make some analysis under the simplified conditions. After the simple analysis we present numerical results with

*nakajima@iae.kyoto-u.ac.jp

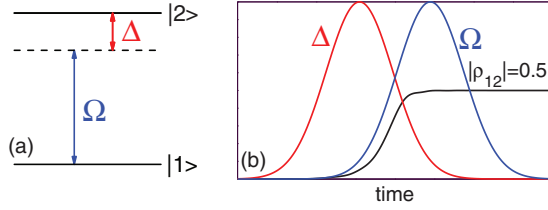


FIG. 1. (Color online) Prototype of the D-STIRAP scheme in a two-level system. With a counterintuitive time sequence of the detuning and pump pulse, stable and maximum coherence is generated.

some typical parameters and then with the precise parameters of Na.

Finally we note that our study on the D-STIRAP with single-photon excitation may be easily extended to the D-STIRAP with two-photon excitation. This implies that the present work is relevant to efficiently generate VUV-XUV light through the FWM processes [12] in which the hyperfine structure of the involved states are not spectrally resolved by the employed laser pulses.

II. FOUR-LEVEL SYSTEM AND GENERALIZED BLOCH EQUATIONS

The level schemes we consider are shown in Fig. 2. They consist of the $3^2S_{1/2}$ and $3^2P_{1/2}$ states of ^{23}Na . Due to the presence of nuclear spin $3/2$, each state has a hyperfine structure. By taking into account the selection rule of dipole transitions, we arrive at the schemes shown in Figs. 2(a) and 2(b) for the cases of linearly and left-circularly polarized pump pulses, respectively. The use of the right-circularly polarized pump pulse leads to the scheme similar to that of

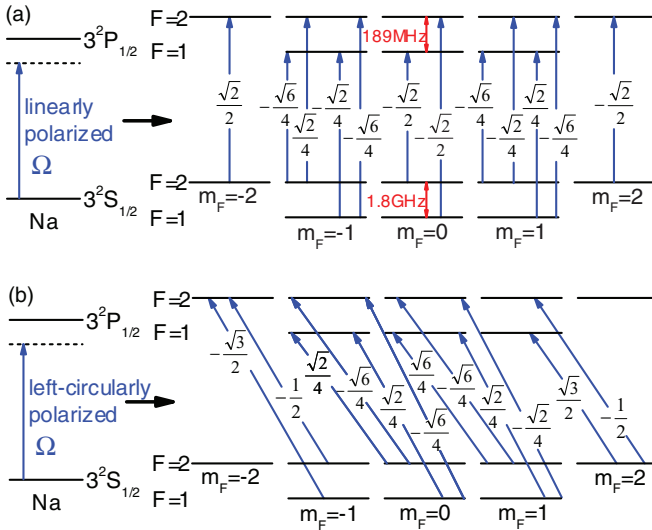


FIG. 2. (Color online) Level schemes considered in this work. The $3^2S_{1/2}$ and $3^2P_{1/2}$ states of ^{23}Na are coupled by the near-resonant pump pulse with (a) linear or (b) left-circular polarization. Scheme (a) consists of the two-level and double- Λ subsystems, while scheme (b) consists of the V, Λ , and double- Λ subsystems. The numbers written in each scheme represent the relevant angular coefficients for the corresponding dipole moments.

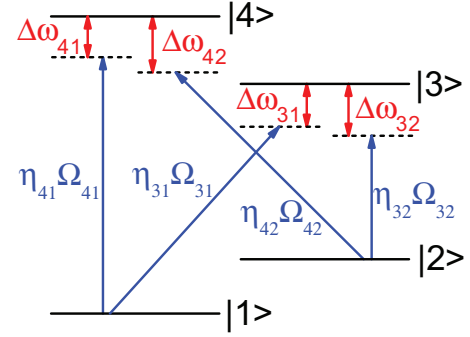


FIG. 3. (Color online) Four-level system. By properly setting the coupling coefficients, η_{ji} , to 0 or 1, the four-level system can be reduced to the two-level, V, Λ , and double- Λ subsystems which appear in Fig. 2.

using the left-circularly polarized pump pulse, and we do not discuss it here. A closer look at the schemes reveals that the entire system consists of several independent subsystems such as two-level, V, Λ , and double- Λ subsystems. The numbers written in Fig. 2 are the relevant angular coefficients for the corresponding dipole moments.

Since both $3^2S_{1/2}$ and $3^2P_{1/2}$ states split into the two hyperfine sublevels, any one of the four subsystems mentioned above is a special case of the most general four-level system, which consists of the two hyperfine sublevels of $3^2S_{1/2}$ and those of $3^2P_{1/2}$. Therefore we now focus on the four-level system as shown in Fig. 3. In this four-level system, all possible dipole couplings and the corresponding detunings are taken into account. η_{ji} in Fig. 3 represents the coupling coefficient for the dipole transition between the lower state i and upper state j . By properly setting η_{ji} to 0 or 1 we can reduce the four-level system to the two-level, V, Λ , or double- Λ subsystems.

The equation of motion of the four-level system shown in Fig. 3 can be described by the Liouville equation,

$$i\hbar\dot{\rho} = [H, \rho], \quad (1)$$

in which H is the total Hamiltonian and ρ is a density operator. More explicitly H can be written, after the rotating-wave approximation, as

$$H = \hbar \begin{pmatrix} 0 & 0 & \eta_{31}\Omega_{31} & \eta_{41}\Omega_{41} \\ 0 & \omega_{21} & \eta_{32}\Omega_{32} & \eta_{42}\Omega_{42} \\ \eta_{31}\Omega_{31} & \eta_{32}\Omega_{32} & \Delta\omega_{31} & 0 \\ \eta_{41}\Omega_{41} & \eta_{42}\Omega_{42} & 0 & \Delta\omega_{41} \end{pmatrix}, \quad (2)$$

where $\Omega_{ji} = \mu_{ji}E(t)/2\hbar$ is the Rabi frequency between states $|i\rangle$ and $|j\rangle$ with μ_{ji} and $E(t)$ being the corresponding dipole moment and the envelope of the electric field of the pump pulse, respectively. Without a loss of generality we assume that Ω_{ji} is a real number. ω_{21} represents the hyperfine splitting of the lower state, and $\Delta\omega_{ji}$ is the detuning of the pump pulse with respect to the transition frequency, ω_{ji} , for the dipole transition between $|i\rangle$ and $|j\rangle$. Note that we do not take into account any decay from the upper states due to the spontaneous decay and ionization loss, so that we can obtain simple expressions which are of great help to understand the

dynamics. Using Eqs. (1) and (2), we obtain the set of density matrix equations, which reads

$$\begin{aligned}
 \dot{\rho}_{11} &= -i\eta_{31}\Omega_{31}(\rho_{31} - \rho_{13}) - i\eta_{41}\Omega_{41}(\rho_{41} - \rho_{14}), \\
 \dot{\rho}_{22} &= -i\eta_{32}\Omega_{32}(\rho_{32} - \rho_{23}) - i\eta_{42}\Omega_{42}(\rho_{42} - \rho_{24}), \\
 \dot{\rho}_{33} &= -i\eta_{31}\Omega_{31}(\rho_{13} - \rho_{31}) - i\eta_{32}\Omega_{32}(\rho_{23} - \rho_{32}), \\
 \dot{\rho}_{44} &= -i\eta_{41}\Omega_{41}(\rho_{14} - \rho_{41}) - i\eta_{42}\Omega_{42}(\rho_{24} - \rho_{42}), \\
 \dot{\rho}_{12} &= i\omega_{21}\rho_{12} + i\eta_{32}\Omega_{32}\rho_{13} + i\eta_{42}\Omega_{42}\rho_{14} \\
 &\quad - i\eta_{31}\Omega_{31}\rho_{32} - i\eta_{41}\Omega_{41}\rho_{42}, \\
 \dot{\rho}_{13} &= i\Delta\omega_{31}\rho_{13} - i\eta_{31}\Omega_{31}(\rho_{33} - \rho_{11}) + i\eta_{32}\Omega_{32}\rho_{12} \\
 &\quad - i\eta_{41}\Omega_{41}\rho_{43}, \\
 \dot{\rho}_{14} &= i\Delta\omega_{41}\rho_{14} - i\eta_{41}\Omega_{41}(\rho_{44} - \rho_{11}) + i\eta_{42}\Omega_{42}\rho_{12} \\
 &\quad - i\eta_{31}\Omega_{31}\rho_{34}, \\
 \dot{\rho}_{23} &= i\Delta\omega_{32}\rho_{23} - i\eta_{32}\Omega_{32}(\rho_{33} - \rho_{22}) + i\eta_{31}\Omega_{31}\rho_{21} \\
 &\quad - i\eta_{42}\Omega_{42}\rho_{43}, \\
 \dot{\rho}_{24} &= i\Delta\omega_{42}\rho_{24} - i\eta_{42}\Omega_{42}(\rho_{44} - \rho_{22}) + i\eta_{41}\Omega_{41}\rho_{21} \\
 &\quad - i\eta_{32}\Omega_{32}\rho_{34}, \\
 \dot{\rho}_{34} &= i\omega_{43}\rho_{34} + i\eta_{41}\Omega_{41}\rho_{31} - i\eta_{31}\Omega_{31}\rho_{14} \\
 &\quad + i\eta_{42}\Omega_{42}\rho_{32} - i\eta_{32}\Omega_{32}\rho_{24}, \tag{3}
 \end{aligned}$$

where ω_{43} represents the hyperfine splitting of the upper state, and $\Delta\omega_{32} = \Delta\omega_{31} - \omega_{21}$ and $\Delta\omega_{42} = \Delta\omega_{41} - \omega_{21}$.

We note that the four kinds of coherence exist in the four-level system, i.e., ρ_{31} , ρ_{32} , ρ_{41} , and ρ_{42} , and obviously they evolve differently in time. Our interest, however, is how much coherence can be generated *in total* between hyperfine manifolds of states $3^2S_{1/2}$ and $3^2P_{1/2}$. Therefore we now recast the set of density matrix equations, Eq. (3), into the generalized Bloch equations by introducing some convenient parameters. For this purpose we first consider the expression of atomic polarization. The atomic polarization of the four-level system under consideration is written as

$$P = \sum_{j,i} \eta_{ji} \mu_{ji} \rho_{ji}. \tag{4}$$

If we regard the four-level system as a generalized two-level system in which the lower and upper states have hyperfine structures, it is natural to define the atomic polarization by

$$P = |\mu_{\text{eff}}| \rho_{\text{eff}}, \tag{5}$$

where μ_{eff} and ρ_{eff} , respectively, are the effective dipole moment and the effective coherence term between the lower and upper state manifolds. If we define μ_{eff} as $|\mu_{\text{eff}}| = \sqrt{\sum_{j,i} (\eta_{ji} \mu_{ji})^2}$, then we notice that ρ_{eff} should be written, from the comparison of the right-hand sides of Eqs. (4) and (5), as

$$\rho_{\text{eff}} = \sum_{j,i} \eta_{ji} A_{ji} \rho_{ji}, \tag{6}$$

in which $A_{ji} = \mu_{ji}/|\mu_{\text{eff}}|$. Note that $|\mu_{\text{eff}}|$ simply serves as a normalization factor for μ_{ji} . We point out that the effective coherence term, ρ_{eff} , may have an opposite sign from those of ρ_{31} , ρ_{32} , ρ_{41} , and ρ_{42} , because we have assumed that the

effective dipole moment, $|\mu_{\text{eff}}|$, is always positive, although it may not necessarily be so. The sign of the coherence term, ρ_{eff} , however, does not influence the observable quantity, since it is simply a matter of the choice of the phase factor.

By recalling that the Bloch equations consist of the three variables, namely, the population inversion term and the real and imaginary coherence terms, we can recast Eq. (3) for the four-level system into the generalized Bloch equations for the effective two-level system with the aid of Eq. (6), which describes the effective complex (real plus imaginary) coherence term. They read

$$\dot{W}_{\text{eff}} = -i\Omega_{\text{eff}}(\rho_{\text{eff}}^* - \rho_{\text{eff}}), \tag{7}$$

$$\dot{\rho}_{\text{eff}}^* = i\Delta\omega_{32}\rho_{\text{eff}}^* - \frac{1}{2}i\Omega_{\text{eff}}W_{\text{eff}} + f_1 + f_2,$$

in which $W_{\text{eff}} (= \rho_{jj} - \rho_{ii})$ and $\Omega_{\text{eff}} (= |\mu_{\text{eff}}|E(t)/\hbar)$ represent the effective population inversion and effective Rabi frequency of the effective two-level system. ρ_{eff}^* is a complex conjugate of ρ_{eff} . Note that Ω_{ji} in Eq. (3) and Ω_{eff} are connected through the relation of $\Omega_{ji} = A_{ji}\Omega_{\text{eff}}/2$. By comparing with the ordinary Bloch equations, we notice that the two additional terms, f_1 and f_2 , appear in Eq. (7). They read

$$\begin{aligned}
 f_1 &= i\omega_{21}(\eta_{31}A_{31}\rho_{13} + \eta_{41}A_{41}\rho_{14}) \\
 &\quad + i\omega_{43}(\eta_{41}A_{41}\rho_{14} + \eta_{42}A_{42}\rho_{24}) \tag{8}
 \end{aligned}$$

and

$$f_2 = -\frac{1}{2}i\Omega_{\text{eff}}f_3, \tag{9}$$

where

$$\begin{aligned}
 f_3 &= -(\eta_{41}A_{41}^2 + \eta_{42}A_{42}^2)\rho_{33} - (\eta_{31}A_{31}^2 + \eta_{32}A_{32}^2)\rho_{44} \\
 &\quad + (\eta_{32}A_{32}^2 + \eta_{42}A_{42}^2)\rho_{11} + (\eta_{31}A_{31}^2 + \eta_{41}A_{41}^2)\rho_{22} \\
 &\quad - (\eta_{31}\eta_{32}A_{31}A_{32} + \eta_{41}\eta_{42}A_{41}A_{42})(\rho_{12} + \rho_{21}) \\
 &\quad + (\eta_{31}\eta_{41}A_{31}A_{41} + \eta_{32}\eta_{42}A_{32}A_{42})(\rho_{34} + \rho_{43}). \tag{10}
 \end{aligned}$$

It is very important to note that the time derivative of f_3 reads

$$\begin{aligned}
 \dot{f}_3 &= -i\omega_{21}(\eta_{31}\eta_{32}A_{31}A_{32} + \eta_{41}\eta_{42}A_{41}A_{42})(\rho_{12} - \rho_{21}) \\
 &\quad - i\omega_{43}(\eta_{31}\eta_{41}A_{31}A_{41} + \eta_{32}\eta_{42}A_{32}A_{42})(\rho_{34} - \rho_{43}) \\
 &\quad + i\Omega_{\text{eff}}(\eta_{32}\eta_{41}\eta_{42}A_{32}A_{41}A_{42} - \eta_{31}\eta_{42}A_{31}A_{42}^2) \\
 &\quad \times (\rho_{31} - \rho_{13}) \\
 &\quad + i\Omega_{\text{eff}}(\eta_{32}\eta_{41}A_{32}^2A_{41} - \eta_{31}\eta_{32}\eta_{42}A_{31}A_{32}A_{42}) \\
 &\quad \times (\rho_{14} - \rho_{41}) \\
 &\quad + i\Omega_{\text{eff}}(\eta_{31}\eta_{41}\eta_{42}A_{31}A_{41}A_{42} - \eta_{32}\eta_{41}A_{32}A_{41}^2) \\
 &\quad \times (\rho_{32} - \rho_{23}) \\
 &\quad + i\Omega_{\text{eff}}(\eta_{31}\eta_{32}\eta_{41}A_{31}A_{32}A_{41} - \eta_{31}\eta_{42}A_{31}^2A_{42}) \\
 &\quad \times (\rho_{42} - \rho_{24}), \tag{11}
 \end{aligned}$$

which will be frequently used in the following analysis.

III. DISCUSSION

In this section we discuss the behavior of the four-level system shown in Fig. 3 through the simple analysis as well as the numerical calculations to solve the set of density matrix

equations given by Eq. (3). In order to obtain the simple expressions and clear physical picture thereby, we perform the analysis for the case in which all the hyperfine splittings are zero, i.e., degenerate hyperfine structure. Such an assumption is lifted later in this section when we resort to the numerical calculations to solve Eq. (3). As expected, the simple analysis turns out to be very helpful to understand the numerical results.

A. Analysis of the four-level system with degenerate hyperfine structure

Although Eqs. (3) and (7) are mathematically equivalent, it is more convenient to use the generalized Bloch equations given by Eq. (7) to carry out the analysis of the four-level system. To simplify the expressions for maximum clarity, we assume, for a moment, that all the hyperfine splittings are zero, i.e., $\omega_{21} = \omega_{43} = 0$. This means that Eq. (8) is reduced to

$$f_1 = 0. \quad (12)$$

In the following, we consider the special case of the four-level system by appropriately setting various η 's to 0 or 1 to reduce the system to the two-level, V, Λ , and double- Λ subsystems, which appear in the schemes shown in Fig. 2.

1. Two-level subsystem

The prototype of the D-STIRAP scheme has been studied in the two-level system, and its behavior is well understood [25]. Nevertheless, we start our analysis with a two-level subsystem to demonstrate the validity of the generalized Bloch equations and our analysis.

If we set one of the four η 's in Fig. 3 to 1 while all others are set to 0, the four-level system is reduced to the two-level subsystem. As a first case, we now set $\eta_{42} = 1$, while $\eta_{31} = \eta_{32} = \eta_{41} = 0$ so that the two-level subsystem is realized by states $|2\rangle$ and $|4\rangle$. Then, from Eq. (11), we find that $\dot{f}_3 = 0$, and hence f_3 is a constant at all time. By referring to Eq. (9) we notice that the value of f_2 also remains the same with that at $t = 0$. If the initial condition is $\rho_{22} = 1$, then, from Eqs. (9) and (10) we obtain

$$f_2 = 0. \quad (13)$$

By substituting Eqs. (12) and (13) into Eq. (7), we find that the generalized Bloch equations are now reduced to the standard Bloch equations for the two-level system. Obviously, if the pulse sequence of the D-STIRAP is applied to the two-level subsystem, we know that $|\rho_{\text{eff}}| = 0.5$.

2. V subsystem

As a second case, we now set $\eta_{32} = \eta_{42} = 1$ and $\eta_{31} = \eta_{41} = 0$ to form the V subsystem by states $|2\rangle$, $|3\rangle$, and $|4\rangle$. From Eq. (11), we again find that $\dot{f}_3 = 0$. If the initial condition is again $\rho_{22} = 1$, then, from Eqs. (9) and (10) we obtain

$$f_2 = 0. \quad (14)$$

This indicates that the generalized Bloch equations for the V subsystem still look the same as the standard Bloch equations for the two-level system. This implies that, if the pulse sequence of the D-STIRAP is applied to the V subsystem, the maximum effective coherence will be $|\rho_{\text{eff}}| = 0.5$.

3. Λ subsystem

As a third case, we set $\eta_{41} = \eta_{42} = 1$ and $\eta_{31} = \eta_{32} = 0$, which reduces the four-level system into the Λ subsystem formed by states $|1\rangle$, $|2\rangle$, and $|4\rangle$. As in the case of the V subsystem, we find that $\dot{f}_3 = 0$ from Eq. (11). However, the natural initial condition for this case is $\rho_{11} = \rho_{22} = 0.5$, and hence $f_2 \neq 0$ as we see from Eqs. (9) and (10). Namely,

$$\begin{aligned} f_2 &= -\frac{1}{2}i\Omega_{\text{eff}}(A_{42}^2\rho_{11} + A_{41}^2\rho_{22}) \\ &= -\frac{1}{4}i\Omega_{\text{eff}}. \end{aligned} \quad (15)$$

Now the generalized Bloch equations read

$$\begin{aligned} \dot{W}'_{\text{eff}} &= -i\Omega_{\text{eff}}(\rho_{\text{eff}}^* - \rho_{\text{eff}}), \\ \dot{\rho}_{\text{eff}}^* &= i\Delta\omega_{32}\rho_{\text{eff}}^* - \frac{1}{2}i\Omega_{\text{eff}}W'_{\text{eff}}, \end{aligned} \quad (16)$$

where $W'_{\text{eff}} = W_{\text{eff}} + \frac{1}{2}$. Note that these equations are identical to the standard Bloch equations for the two-level system. This means that if the pulse sequence of the D-STIRAP is applied to this subsystem, the initial value of the population inversion term, W'_{eff} , is completely transferred to the real part of the coherence term, $\text{Re}(\rho_{\text{eff}})$, i.e., $W'_{\text{eff}} \rightarrow 2\text{Re}(\rho_{\text{eff}})$. Since the initial value of W_{eff} is -1 for this case, $W'_{\text{eff}} = -\frac{1}{2}$, and $\text{Re}(\rho_{\text{eff}}) = -\frac{1}{4}$. Consequently, the degree of effective coherence is $|\rho_{\text{eff}}| = 0.25$, which is only half of the values for the two-level and V subsystems.

4. Double- Λ subsystem

We can continue the similar analysis for the double- Λ subsystem by setting $\eta_{31} = \eta_{41} = \eta_{32} = \eta_{42} = 1$. If we look into Eq. (11) carefully, we notice that the common term of $B = A_{31}A_{42} - A_{32}A_{41}$ appears frequently. Depending on the specific values of A_{31} , A_{42} , A_{32} , and A_{41} , B may be zero or nonzero, and we consider those two cases separately.

The first case of $B = 0$ is very similar to the case of Λ subsystem, and $\dot{f}_3 = 0$ from Eq. (11). If we assume the most natural initial condition of $\rho_{11} = \rho_{22} = 0.5$, then, f_2 is found, from Eqs. (9) and (10), as

$$f_2 = -\frac{1}{4}i\Omega_{\text{eff}}. \quad (17)$$

Following the argument we have made for the Λ subsystem, we can conclude that $|\rho_{\text{eff}}| = 0.25$.

The second case of $B \neq 0$ is different, because $\dot{f}_3 \neq 0$. As a result, f_2 cannot be expressed in a simple form, which means that we cannot obtain a simple analytical result for $|\rho_{\text{eff}}|$.

B. Numerical calculations

Having clarified the attainable degree of coherence in the four kinds of subsystems, we now numerically solve the set of density matrix equations described in Eq. (3) and estimate the degree of effective coherence defined by Eq. (6). In order to connect the previous analysis for the case of degenerate hyperfine structure and the numerical results to be presented here, we perform numerical calculations for the cases of both degenerate and nondegenerate hyperfine structures.

The coupling coefficients such as $\eta_{ji}\Omega_{ji}$ we need to solve Eq. (3) for Fig. 3 are taken from those given in Fig. 2 for the Na atom. Accordingly, the states $|1\rangle$ and $|2\rangle$ ($|3\rangle$ and $|4\rangle$)

in Fig. 3 should be read as the $F = 1$ and $F = 2$ states of $3^2S_{1/2}$ ($3^2P_{1/2}$). Note that the different magnetic sublevels of the hyperfine states have to be appropriately chosen for the different subsystems. For all calculations presented in this paper we introduce two pulses, i.e., the off-resonant and resonant pulses. The former serves as the detuning pulse through ac Stark shifts which result in the time-dependent detuning of $\Delta_{\text{eff}}(t)$, and the latter serves as the pump pulse with the effective Rabi frequency of $\Omega_{\text{eff}}(t)$. If we assume that both pulses have Gaussian temporal shapes, they can be written as

$$\Delta_{\text{eff}}(t) = \Delta_0 \exp\left[-\ln 4 \left(\frac{t}{\tau_\Delta}\right)^2\right] + \delta_0 \quad (18)$$

and

$$\Omega_{\text{eff}}(t) = \Omega_{\text{eff}}^0 \exp\left[-\frac{1}{2} \ln 4 \left(\frac{t - t_{\text{delay}}}{\tau_\Omega}\right)^2\right]. \quad (19)$$

In these equations, Δ_0 and Ω_{eff}^0 represent the peak amplitudes of the detuning pulse and the effective Rabi frequency, respectively. t_{delay} is the time delay between the two pulses, and δ_0 stands for the initial detuning of the pump pulse with respect to the transition frequency ω_{32} between $|2\rangle$ and $|3\rangle$. τ_Δ and τ_Ω , respectively, are the durations of the detuning and pump pulses defined for the intensity. Note that the additional factor of $1/2$ in front of $\ln 4$ appears only in Eq. (19), since the Rabi frequency is defined for the field amplitude. In our case we have set them to be $\tau_\Delta = \sqrt{2}\tau_\Omega = 1$. In the following calculations, all the parameters are chosen with respect to τ_Δ . The time delay t_{delay} is defined in the unit of τ_Δ while other parameters such as Δ_0 , Ω_{eff}^0 , δ_0 , and also the hyperfine splittings ω_{21} , ω_{43} , are defined in units of $1/\tau_\Delta$.

1. Degenerate hyperfine structure

We first assume that all the hyperfine splittings are zero, i.e., $\omega_{21} = \omega_{43} = 0$. Then, all the detunings in Eq. (3) are solely induced by the detuning pulse, i.e., $\Delta\omega_{ji} = \Delta_{\text{eff}}(t)$. Under such an assumption we find that the numerical solutions agree well with the previous analysis, which again confirms the correctness of our treatment using the generalized Bloch equations.

In Fig. 4 we show the color-coded plot of the variation of the degree of effective coherence for the two-level and V subsystems under the D-STIRAP pulse sequence. The former subsystem is realized by choosing $|3^2S_{1/2} F = 2, m_F = -2\rangle$ and $|3^2P_{1/2} F = 2, m_F = -2\rangle$ as $|2\rangle$ and $|4\rangle$, respectively, for which $A_{42} = 1$. The latter subsystem is realized by choosing $|3^2S_{1/2} F = 2, m_F = 2\rangle$, $|3^2P_{1/2} F = 1, m_F = 1\rangle$, and $|3^2P_{1/2} F = 2, m_F = 1\rangle$ as $|2\rangle$, $|3\rangle$, and $|4\rangle$, respectively, for which $A_{32} = \frac{\sqrt{3}}{2}$ and $A_{42} = -\frac{1}{2}$. Figures 4(a) and 4(b) clearly show, respectively, that the results are identical for both subsystems. Under the parameter range which satisfies the adiabaticity of D-STIRAP, the degree of effective coherence reaches 0.5, and it is reasonably robust against the changes of Ω_{eff}^0 and Δ_0 [Fig. 4(a)]. A similar relation is true for the changes of t_{delay} and δ_0 [Fig. 4(b)].

We make similar plots for the Λ and double- Λ subsystems. The results are shown in Fig. 5. The former subsystem is realized by choosing $|3^2S_{1/2} F = 1, m_F = -1\rangle$,

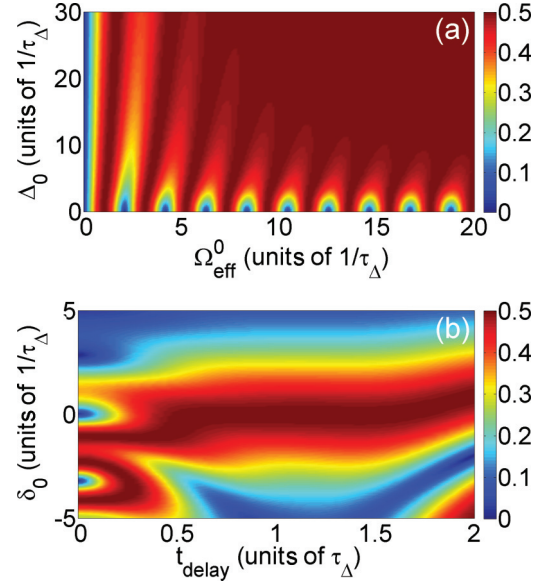


FIG. 4. (Color online) Color-coded plot of the variation of the degree of effective coherence, $|\rho_{\text{eff}}|$, in two-level and V subsystems as functions of (a) effective Rabi frequency, Ω_{eff}^0 , and detuning, Δ_0 , with $t_{\text{delay}} = 1.5\tau_\Delta$ and $\delta_0 = 0$, and (b) time delay, t_{delay} , and initial detuning, δ_0 , with $\Omega_{\text{eff}}^0 = 15/\tau_\Delta$ and $\Delta_0 = 20/\tau_\Delta$. Note that the results in graphs (a) and (b) are respectively identical for both subsystems.

$|3^2S_{1/2} F = 2, m_F = -1\rangle$, and $|3^2P_{1/2} F = 2, m_F = -2\rangle$ as $|1\rangle$, $|2\rangle$, and $|4\rangle$, for which $A_{41} = -\frac{\sqrt{3}}{2}$ and $A_{42} = -\frac{1}{2}$. The latter subsystem is realized by choosing $|3^2S_{1/2} F = 1, m_F = 0\rangle$, $|3^2S_{1/2} F = 2, m_F = 0\rangle$, $|3^2P_{1/2} F = 1, m_F = -1\rangle$, and $|3^2P_{1/2} F = 2, m_F = -1\rangle$ as $|1\rangle$, $|2\rangle$, $|3\rangle$, and $|4\rangle$, for which $A_{31} = \frac{\sqrt{2}}{4}$, $A_{32} = \frac{\sqrt{2}}{4}$, $A_{41} = -\frac{\sqrt{6}}{4}$, and $A_{42} = -\frac{\sqrt{6}}{4}$, and these

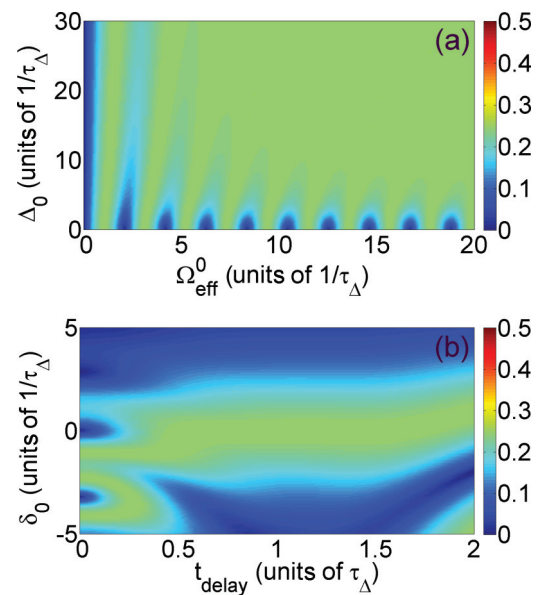


FIG. 5. (Color online) Similar to Fig. 4 but for the Λ and double- Λ subsystems with $B = 0$. Note that the results in graphs (a) and (b) are respectively identical for both subsystems.

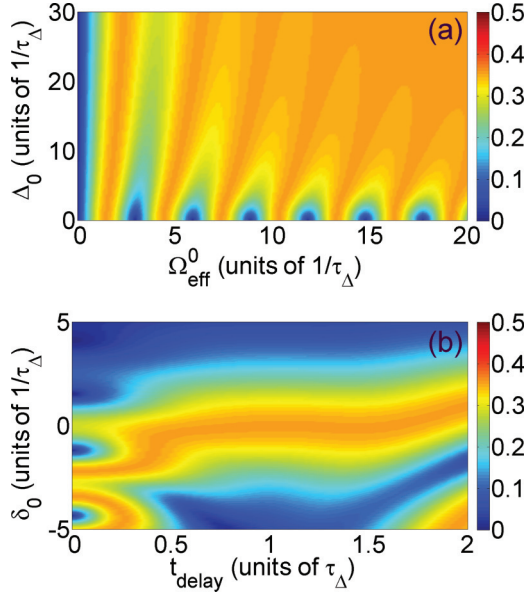


FIG. 6. (Color online) Similar to Fig. 5 but for the double- Λ subsystem with $B = -\frac{1}{2}$.

values of A 's result in $B = 0$. Again, Figs. 5(a) and 5(b) show, respectively, that the results are identical for both subsystems. Note that the pattern of Figs. 4 and 5 are almost the same except for the coloring. Namely, the difference between them arises from the difference of peak values of $|\rho_{\text{eff}}|$: $|\rho_{\text{eff}}| = 0.25$ in Fig. 5, while $|\rho_{\text{eff}}| = 0.5$ in Fig. 4.

As we have found in Sec. III A, the dynamics of the double- Λ subsystem can be different, depending on the values of B , which have been defined as $B = A_{31}A_{42} - A_{32}A_{41}$. In the above example used for Fig. 5, $B = 0$. We now consider the case of $B \neq 0$ for the double- Λ subsystem. It can be realized, for instance, by choosing $|3^2S_{1/2} F = 1, m_F = -1\rangle$, $|3^2S_{1/2} F = 2, m_F = -1\rangle$, $|3^2P_{1/2} F = 1, m_F = -1\rangle$, and $|3^2P_{1/2} F = 2, m_F = -1\rangle$ as $|1\rangle$, $|2\rangle$, $|3\rangle$, and $|4\rangle$, for which $A_{31} = -\frac{\sqrt{2}}{4}$, $A_{32} = -\frac{\sqrt{6}}{4}$, $A_{41} = -\frac{\sqrt{6}}{4}$, and $A_{42} = \frac{\sqrt{2}}{4}$, and consequently $B = -\frac{1}{2}$. The corresponding results are shown in Fig. 6. It turns out that, apart from the coloring, the pattern of the graphs in Fig. 6 is somehow similar to that in Figs. 4 and 5. Moreover, the degree of the effective coherence in Fig. 6 is $|\rho_{\text{eff}}| = 0.35$, which is between the values in Fig. 4 ($|\rho_{\text{eff}}| = 0.5$) and Fig. 5 ($|\rho_{\text{eff}}| = 0.25$). Although we expect to see more difference due to the fact that $f_3 \neq 0$ if $B \neq 0$, it does not seem to be the case, as far as we can notice by comparing Figs. 5 and 6.

2. Nondegenerate hyperfine structure

Now we turn to the more realistic situation where the hyperfine splittings are nonzero. For this case, we do not have to consider the case of the two-level subsystem because of the absence of degeneracy or nondegeneracy and focus on the cases of nondegenerate V, Λ , and double- Λ subsystems.

Representative results are shown in Fig. 7 for $\Delta_0 = 20/\tau_\Delta$, $\Omega_{\text{eff}}^0 = 15/\tau_\Delta$, and $t_{\text{delay}} = 1.5\tau_\Delta$ with the hyperfine splittings chosen to be $\omega_{21} = 0.5/\tau_\Delta$ and $\omega_{43} = 0.05/\tau_\Delta$. Figure 7(a) shows the maximum values of the degree of effective coher-

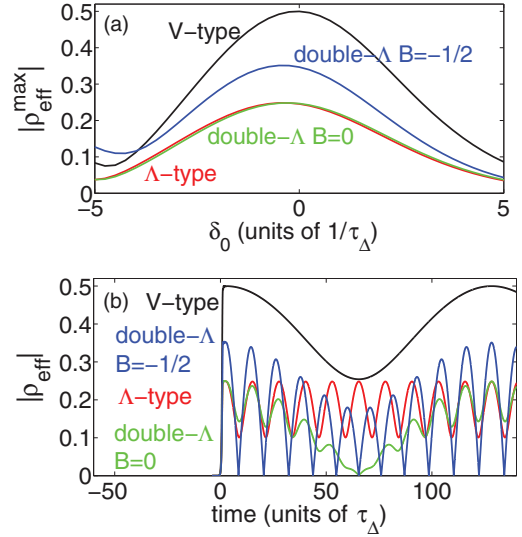


FIG. 7. (Color online) (a) Maximum values of the generated effective coherence, $|\rho_{\text{eff}}^{\text{max}}|$, as a function of initial detuning, δ_0 . (b) Time evolution of effective coherence, $|\rho_{\text{eff}}|$, with the best choice of initial detunings for the nondegenerate V, Λ , and double- Λ subsystems. The employed parameters are $\Delta_0 = 20/\tau_\Delta$, $\Omega_{\text{eff}}^0 = 15/\tau_\Delta$, and $t_{\text{delay}} = 1.5\tau_\Delta$.

ence, $|\rho_{\text{eff}}^{\text{max}}|$, as a function of initial detuning, δ_0 , for the V, Λ , and double- Λ subsystems. In particular the results with $B = 0$ and $B \neq 0$ are both shown for the double- Λ subsystem.

What we can learn from Fig. 7(a) is that the value of δ_0 has to be carefully chosen to maximize the value of $|\rho_{\text{eff}}^{\text{max}}|$, and the best choice of δ_0 is always at the slightly negative side of $\delta_0 = 0$ for all subsystems; i.e., the pump laser frequency must be between the two transition frequencies of the subsystems. We also notice that the best value of δ_0 for the case of the V subsystem is closer to 0 compared with those of Λ and double- Λ , simply because the hyperfine structure that matters for the former is that of the upper state and hence the hyperfine splitting is much smaller than that of the lower state, while it is that of the lower states for the latter.

In Fig. 7(b), we plot the time evolution of the degree of effective coherence for different subsystems at the best choice of initial detuning. The degree of effective coherence modulates with the frequencies which are essentially determined by the hyperfine splittings of the lower and upper state manifolds. This is simply because the time evolution of effective coherence is a collective result of the four coherence terms, ρ_{31} , ρ_{32} , ρ_{41} , and ρ_{42} , as we see in Eq. (6). Figure 7(b) also shows that, apart from the modulations due to the presence of nonzero hyperfine splittings, the maximum values of $|\rho_{\text{eff}}|$ do not exceed the values predicted in Sec. III A, which have been obtained by assuming the zero hyperfine splittings.

We repeat the similar calculations for the time evolution of the degree of effective coherence with different values of the amplitudes of the detuning pulse, Δ_0 , Rabi frequency, Ω_{eff}^0 , and time delay, t_{delay} . The results (not shown here) imply that the time evolution of the degree of effective coherence is not very sensitive to the variations of these parameters, which is similar to the cases of Figs. 4–6.

C. Application to the D_1 transition of Na

Finally we perform calculations for the entire D_1 transition of the Na atom shown in Fig. 2. This means that we now deal the entire system, which contains several different subsystems discussed before. To quantify the degree of effective coherence in the Na system (Fig. 2), we introduce a new variable, $\rho_{\text{eff}}^{\text{Na}}$, which is defined by

$$|\rho_{\text{eff}}^{\text{Na}}| = \frac{\sum_k P_k |\rho_{\text{eff}}^k|}{\sum_k P_k}, \quad (20)$$

where P_k is the population in the lower ($F = 1$ and 2 hyperfine) states and $|\rho_{\text{eff}}^k|$ is the generated effective coherence in the subsystem denoted as k .

In the calculations we assume a linearly polarized pulse at the wavelength of 1064 nm to induce the time-dependent Stark shift, which serves as the detuning pulse. As for the pump pulse, we assume a transform-limited pulse with linear or left-circular polarization at the wavelength of 589 nm to be resonant with the D_1 transition. As in Sec. III B, we assume that both detuning and pump pulses have Gaussian temporal shapes, and their durations are set to be 10 ps (for the full width at half maximum of their pulse intensities). The bandwidth of the 10 ps pump pulse is sufficiently broad to be resonant with all hyperfine transitions associated with the D_1 transition, while the D_2 transition, $3^2S_{1/2} \rightarrow 3^2P_{3/2}$, is still far away from resonance.

We note that the amount of the Stark shifts induced by the same detuning pulse are generally different for different hyperfine sublevels within the same hyperfine manifold. However, for the hyperfine manifold with total angular momentum of $J = \frac{1}{2}$, the amount of Stark shifts is exactly the same for all hyperfine sublevels [33,34]. By making use of the equations and values reported in Refs. [33,34], we can write the effective detuning induced by the detuning pulse as

$$\Delta_{\text{eff}}(\text{rad/s}) \approx 201 I_{\text{det}}(\text{W/cm}^2), \quad (21)$$

for all hyperfine sublevels in the ground state, where I_{det} is the detuning pulse intensity. In order to satisfy the adiabatic condition, it is chosen as $I_{\text{det}} = 10 \text{ GW/cm}^2$. The hyperfine splittings of states $3^2S_{1/2}$ and $3^2P_{1/2}$ are 1.8 GHz and 189 MHz, respectively, and they are much smaller compared with the magnitudes of the effective detunings induced by the detuning pulse. This means that $\Delta\omega_{ji} \simeq \Delta_{\text{eff}}$ in Eq. (3) when the pump pulse is on. The effective transition dipole moment between states $3^2S_{1/2}$ and $3^2P_{1/2}$ is $\mu_{\text{eff}} \approx 3 \times 10^{-29} \text{ C m}$ taken on Ref. [34], and accordingly we can write the effective Rabi frequency as

$$\Omega_{\text{eff}}(\text{rad/s}) = 8.2 \times 10^8 \sqrt{I_{\text{pump}}(\text{W/cm}^2)}, \quad (22)$$

in which I_{pump} is the pump pulse intensity and we set it at $I_{\text{pump}} = 3.3 \text{ MW/cm}^2$. We adjust the time delay between the detuning pulse and the pump pulse to be $t_{\text{delay}} = 10 \text{ ps}$. For completeness, we also include the spontaneous lifetime of the excited $3p$ state, which is about 16 ns.

In Fig. 8 we show the time evolution of the degree of coherence, $|\rho_{\text{eff}}^{\text{Na}}|$, in the Na atom for the linearly and left-circularly polarized pump pulse. Just after the pump pulse the degree of coherence takes the largest value, which is more than 0.4 for the linearly polarized pump pulse, since the dephasing

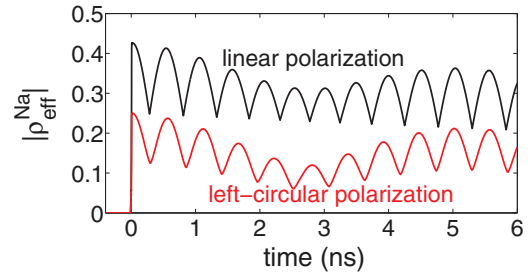


FIG. 8. (Color online) Time evolution of the degree of coherence, $|\rho_{\text{eff}}^{\text{Na}}|$, for the linearly (black) and left-circularly (red) polarized pump pulse.

originating from the hyperfine splittings is negligible at this time scale. As the time passes, however, the dephasing and rephasing of coherence takes place. The slow modulation we see in Fig. 8 is due to the hyperfine splittings of the upper states. We also note that the lifetime of the upper states hardly plays a role in the time scale presented in Fig. 8. Although we cannot obtain stable coherence in this realistic case due to the presence of nonzero hyperfine splittings, as we have already learned in Sec. III A, we can still say that the average value of the degree of coherence is about 0.3 for the linearly polarized pump pulse. The result for the left-circularly polarized pump pulse is worse and it cannot be better than 0.15. The reason for this difference is clear if we look at Fig. 2 once more: For the linearly polarized pump pulse [Fig. 2(a)], four of the subsystems are two-level ones in which the degree of coherence reaches the possible maximum value of 0.5, and two of the subsystems are double- Λ ones with $B = -\frac{1}{2}$ and hence the degree of coherence can be 0.35. For the left-circular pump pulse [Fig. 2(b)], none of the subsystems are two-level ones, and there is only one V subsystem, one Λ subsystem, and two double- Λ subsystems with $B = 0$. It is clear that the performance of the latter case is not as good as that of the former case. As we have already seen in Figs. 4–6, none of the subsystems are sensitive to the pump pulse intensity, detuning pulse intensity, initial detuning, and time delay between the pump and detuning pulses. Accordingly the entire system (which is a sum of the subsystems) is not sensitive to those parameters either. As for the sensitivity of the degree of generated coherence to the Doppler broadening, we can see from Fig. 7(a) that it is essentially determined by the laser pulse duration irrespective of the kind of employed atoms. For the 10-ps pulses we have assumed here, the Doppler shift as large as 10 GHz will not influence the result. Since the Doppler broadening of the Na atomic vapor at room temperature is only $\sim 1 \text{ GHz}$, we may safely neglect it.

IV. CONCLUSIONS

In conclusion we have theoretically studied the generation of coherence in generalized two-level atoms with hyperfine structure by using the D-STIRAP pulse sequence. We have found that the degree of attainable coherence between the ground- and excited-state manifold cannot be as large as that in ideal two-level atoms, which is somehow expected without any calculations. However, we have also found that the substantial degree of coherence can still be produced in real atoms (such as Na) with small modulations, where the modulation

periods are essentially determined by the hyperfine splittings of the ground and excited states. We have also demonstrated the robustness of the D-STIRAP scheme in atoms with hyperfine structure against the various parameters such as the pump pulse intensity, detuning pulse intensity, initial detuning, time delay between the two pulses, and Doppler broadening.

To be most specific we have also presented the results for the D_1 transition of Na with hyperfine structure. Similar results should be obtained with other atoms. Our finding would be

a useful benchmark to generate high atomic coherence in real atoms with hyperfine structure toward applications in nonlinear optics.

ACKNOWLEDGMENT

This work was supported by a Grant-in-Aid for Scientific Research from the Ministry of Education and Science of Japan.

-
- [1] S. E. Harris, J. E. Field, and A. Imamoglu, *Phys. Rev. Lett.* **64**, 1107 (1990).
 - [2] S. E. Harris, *Phys. Rev. Lett.* **62**, 1033 (1989).
 - [3] N. V. Vitanov, M. Fleischhauer, B. W. Shore, and K. Bergmann, *Adv. Atom. Mol. Opt. Phys.* **46**, 55 (2001).
 - [4] M. Keyl, *Phys. Rep.* **369**, 431 (2002).
 - [5] M. Jain, H. Xia, G. Y. Yin, A. J. Merriam, and S. E. Harris, *Phys. Rev. Lett.* **77**, 4326 (1996).
 - [6] A. J. Merriam, S. J. Sharpe, H. Xia, D. Manuszak, G. Y. Yin, and S. E. Harris, *Opt. Lett.* **24**, 625 (1999).
 - [7] V. A. Sautenkov, C. Y. Ye, Y. V. Rostovtsev, G. R. Welch, and M. O. Scully, *Phys. Rev. A* **70**, 033406 (2004).
 - [8] S. A. Myslivets, A. K. Popov, T. Halfmann, J. P. Marangos, and T. F. George, *Opt. Commun.* **209**, 335 (2002).
 - [9] T. Rickes, J. P. Marangos, and T. Halfmann, *Opt. Commun.* **227**, 133 (2003).
 - [10] M. Oberst, J. Klein, and T. Halfmann, *Opt. Commun.* **264**, 463 (2006).
 - [11] S. Chakrabarti, H. Muench, and T. Halfmann, *Phys. Rev. A* **82**, 063817 (2010).
 - [12] L. Deng and T. Nakajima, *Opt. Express* **20**, 17566 (2012).
 - [13] R. Buffa, M. P. Anscombe, and J. P. Marangos, *Phys. Rev. A* **67**, 033801 (2003).
 - [14] M. V. Tognetti and R. Buffa, *J. Phys. B* **37**, 1 (2004).
 - [15] R. Buffa, M. V. Tognetti, M. P. Anscombe, and J. P. Marangos, *Phys. Rev. A* **72**, 053811 (2005).
 - [16] R. Mahon, T. J. McIlrath, and D. W. Koopman, *Appl. Phys. Lett.* **33**, 305 (1978).
 - [17] G. Hilber, A. Lago, and R. Wallenstein, *J. Opt. Soc. Am. B* **4**, 1753 (1987).
 - [18] J. P. Marangos, N. Shen, H. Ma, M. H. R. Hutchinson, and J. P. Connerade, *J. Opt. Soc. Am. B* **7**, 1254 (1990).
 - [19] K. S. E. Eikema, J. Walz, and T. W. Hänsch, *Phys. Rev. Lett.* **83**, 3828 (1999).
 - [20] E. Arimondo, *Prog. Opt.* **35**, 257 (1996).
 - [21] N. V. Vitanov, K. A. Suominen, and B. W. Shore, *J. Phys. B* **32**, 4535 (1999).
 - [22] L. Deng, Y. P. Niu, Y. Xiang, S. Q. Jin, and S. Q. Gong, *J. Phys. B* **43**, 035401 (2010).
 - [23] A. A. Soares and L. E. E. de Araujo, *Phys. Rev. A* **76**, 043818 (2007).
 - [24] L. Deng, Y. P. Niu, L. L. Jin, and S. Q. Gong, *J. Phys. B* **43**, 205502 (2010).
 - [25] N. V. Vitanov and B. W. Shore, *Phys. Rev. A* **73**, 053402 (2006).
 - [26] E. A. Korsunsky, T. Halfmann, J. P. Marangos, and K. Bergmann, *Eur. Phys. J. D* **23**, 167 (2003).
 - [27] R. Yamazaki, K. I. Kanda, F. Inoue, K. Toyoda, and S. Urabe, *Phys. Rev. A* **78**, 023808 (2008).
 - [28] Y. Loiko, C. Serrat, R. Vilaseca, V. Ahufinger, J. Mompart, and R. Corbalán, *Phys. Rev. A* **79**, 053809 (2009).
 - [29] F. T. Hioe and C. E. Carroll, *Phys. Rev. A* **37**, 3000 (1988).
 - [30] H. Y. Ling, Y. Q. Li, and M. Xiao, *Phys. Rev. A* **53**, 1014 (1996).
 - [31] H. Xia, S. J. Sharpe, A. J. Merriam, and S. E. Harris, *Phys. Rev. A* **56**, R3362 (1997).
 - [32] L. E. E. de Araujo, *Phys. Rev. A* **69**, 013408 (2004).
 - [33] M. S. Safronova, B. Arora, and C. W. Clark, *Phys. Rev. A* **73**, 022505 (2006).
 - [34] B. Arora, M. S. Safronova, and C. W. Clark, *Phys. Rev. A* **76**, 052509 (2007).